
Unsupervised Program Synthesis for Images using Tree-Structured LSTM

Chenghui Zhou
Carnegie Mellon University
chenghuz@cs.cmu.edu

Chun-Liang Li
Carnegie Mellon University
chunli@cs.cmu.edu

Barnabás Póczos
Carnegie Mellon University
bapocz@cs.cmu.edu

Abstract

Program synthesis has recently emerged as a promising approach to the image parsing task. However, most prior works have relied on supervised learning methods, which require ground truth programs for each training image. We present an unsupervised learning algorithm that can parse constructive solid geometry (CSG) images into context-free grammar with a non-differentiable renderer. We propose a grammar-encoded tree LSTM to effectively constrain our search space by leveraging the structure of the context-free grammar while handling the non-differentiable renderer via REINFORCE and encouraging the exploration by regularizing the objective with an entropy term. Instead of using simple Monte Carlo sampling, we propose a lower-variance entropy estimator with sampling without replacement for effective exploration. We demonstrate the effectiveness of the proposed algorithm on a synthetic 2D CSG dataset, which outperforms baseline models by a large margin.

1 Introduction

Image generation has been an extensively studied topic in machine learning and computer vision. Vast number of papers have explored generating images through low dimensional latent representations [Goodfellow *et al.*, 2014; Arjovsky *et al.*, 2017; Li *et al.*, 2017; Kingma and Welling, 2013; van den Oord *et al.*, 2017; Oord *et al.*, 2016]. However, it is challenging to learn disentangled representations which allows us to control the generation after learning the generative models [Higgins *et al.*, 2017; Kim and Mnih, 2018; Locatello *et al.*, 2018; Chen *et al.*, 2016]. In this paper, we will explore generating constructive solid geometry images through programs in the form of context-free grammar. We can consider these programs as an alternative of low-dimensional representation of the image. The model for extracting the programs can be seen as an encoder and the renderer that reconstructs the image is the decoder. Parsing an image of geometric shapes into programs enables us to manipulate only the desired components of the image while reconstruct the rest of the image.

There are two types of image renderers that construct the images from programs – differentiable and non-differentiable renderers. While creating differentiable renderers is a fast developing field (e.g. [Li *et al.*, 2018; Liu *et al.*, 2019]), they are still not as well-developed as the non-differentiable ones. On the other hand, learning a generative process by combining modern machine learning models (e.g. neural networks) and non-differentiable renderers is challenging because we are not able to obtain the gradient respect to the input.

The goal of our paper is learning to parse an image into programs which can be described by a context-free-grammar, such as constructive solid geometry (CSG) image [Hubbard, 1990]. [Sharma *et al.*, 2018] have studied the same problem using supervised learning where the images and the programs are paired up as the input. However, we want to tackle a more general image parsing problem where the ground truth program is not available for training. In this paper, we aim to solve it with only target images as input without any other form of program supervision.

Here are the three key components to successfully learn to parse an image to programs with minimum data supervision:

- We adopt a **non-differentiable** renderer for this problem. The lack of direct gradient information from the non-differentiable renderer implies that we can only train our model based on the final reconstructed image’s reward. We use REINFORCE [Williams, 1992] as our main building component.
- We introduce **Tree LSTM** to impose a structure on our output space to reduce the search space to only valid programs. A naive parameterization of program generation is using simple RNN, which is not guaranteed to always generate grammatically correct programs. However, the renderer cannot parse invalid programs and the reconstructed images of invalid programs are defined to receive low rewards. Therefore, it is necessary to limit the search space to avoid the sparse reward problem.
- We propose a **better entropy estimator** for the standard entropy regularization to encourage exploration of the search space. We propose a stepwise entropy estimator and show that it has lower variance than the naive estimator. Instead of using simple Monte Carlo, we adopt a **sampling without replacement** scheme to improve the optimization efficiency significantly.

2 Related Work

Our work is related to program synthesis, vision-as-inverse-graphics, as well as generating images with stroke-based rendering (SBR) systems.

Program synthesis has been a growing interest to researchers in machine learning [Balog *et al.*, 2017; Shin *et al.*, 2018; Devlin *et al.*, 2017; Zohar and Wolf, 2018]. Research on converting images to programs are more directly related to our work [Sharma *et al.*, 2018; Ellis *et al.*, 2019; Tian *et al.*, 2019; Ellis *et al.*, 2018; Liu *et al.*, 2018]. The setup of our work closely follows [Sharma *et al.*, 2018] and [Ellis *et al.*, 2019] is also an extension from it. Both works rely on supervised pretraining before using REINFORCE to fine tune the models, while our goal is to train the grammar generation model with only the target images as the inputs without the supervision of the corresponding programs of training images. [Tian *et al.*, 2019] incorporated a differentiable renderer into the learning pipeline while we treated our renderer as an external procedure independent from the learning process. With a non-differentiable renderer, we cannot directly propagate the gradient from the reward to the grammar generation model. This distinction leads to very different algorithm designs. [Liu *et al.*, 2018] focuses on the symmetry and repetition aspects of a scene. The algorithm takes in a scene of 3D geometric objects stacked or lined up and parse it into programs in terms of loops and rotations. Although related, this work has a very different setting from ours. [Ellis *et al.*, 2018] used neural network to extract the shapes from hand-drawn sketches, formulated the grammatical rules as constraints and obtain the final program by solving a constraint satisfaction problem. This process can be computationally expensive compared to neural network’s performance in test time.

Research in vision-as-inverse-graphics concerns parsing a scene into a collection of shapes or 3D primitives with descriptions that imitates the original scene [Tulsiani *et al.*, 2017; Romaszko *et al.*, 2017; Wu *et al.*, 2017]. [Wu *et al.*, 2017] de-renders a scene into a collection of objects, such as a tree and a girl etc, with colors and locations as parameters. [Yao *et al.*, 2018] differs from the last work in that it further manipulates the objects de-rendered, for example, changing a car’s color from blue to red and putting it back to the scene. These works do not deal with the interactions among the parsed objects through operations, which is the distinction with our setting.

Stroke-based rendering creates an image in a way natural to human. Some of the examples are recreating paintings imitating a painter’s brush stroke by [Huang *et al.*, 2019], drawing sketches of objects by [Ha and Eck, 2017]. SPIRAL by [Ganin *et al.*, 2018] is an adversarially trained deep reinforcement learning agent. The agent is able to recreate MuJoCo scenes, MNIST digits, and Omniglot characters. Stroke-based rendering behaves in an additive way. The action space usually consists of a line of various continuous parameters such as width and length. A grammar structure is unnecessary to the rendering process because each action is additive. This contrasts from our problem in which the action space includes primitive shapes, operations as well as grammar tokens. Overall, stroke-based rendering is less expressive and less precise when it comes to structured objects generation.

3 Problem Definition

The input of the model is an image constructed from basic shapes such as triangle, circle or triangle, each with a designated size and location (see Figure 6). The output of the model is a program to reconstruct the input in the format of context-free grammar (CFG).

In this paper, we use constructive solid geometry (CSG) image [Hubbard, 1990] to form an image. Some sample images can be found in Figure 8. The CFG for CSG includes the binary shape operations of plus, minus, and intersection. The context-free grammar rules are as follows:

$$S \rightarrow E \tag{1}$$

$$E \rightarrow EET|P \tag{2}$$

$$T \rightarrow +|-|* \tag{3}$$

$$P \rightarrow SHAPE_1|SHAPE_2|\dots|SHAPE_n. \tag{4}$$

S , T , and P are non-terminal tokens for the start, operations, and shapes. The others are called terminal tokens, such as $+$ (union), $*$ (intersection), $-$ (subtraction), and $c(48, 16, 8)$ stands for a circle with radius 8 and at $(48, 16)$. Each line above is called *production rule* or just *rule* for simplicity. Please refer to Figure 7 for some examples of CSG images with their corresponding programs.

The setting of the problem is adopted from [Sharma *et al.*, 2018]. They are able to parse the grammatical programs from the images through supervised training. However, supervised training involves constructing images with known programs to be the input at the same time. Manually constructing programs for training can be time-consuming but also restricts the target images to be an exact translation of the program. We are interested in unsupervised training because images usually do not come with their corresponding programs.

4 Proposed Algorithm

Our model consists of a CNN encoder for reading the canvas, an embedding layer for the action tokens, and an RNN for generating the grammatical program sequences (see Figure 1 for demonstration). The model was trained with entropy regularized REINFORCE [Williams, 1992]. Let $\mathcal{H}(s)$ be the entropy of the sequence s (we will define this later), $f(s)$ is a reward function based on the sequence, and θ is the parameters of our model. The objective is optimized as follows:

$$\Delta\theta \propto \mathbb{E}_{s \sim p_\theta(s)}[\nabla_\theta \log p(s)f(s)] + \alpha \nabla_\theta \mathcal{H}(s), \tag{5}$$

The output program s is converted to an image \mathbf{y} by a non-differentiable renderer. The image is compared to the target image \mathbf{x} and receives a reward $R(\mathbf{x}, \mathbf{y})$, which is our definition of $f(s)$. We adopt Chamfer distance as part of the reward function as in [Sharma *et al.*, 2018]. Chamfer distance calculates the average matching distance to the nearest feature. Let $x \in \mathbf{x}$ and $y \in \mathbf{y}$ be pixels in each image respectively. Chamfer distance is described formally as follows:

$$Ch(\mathbf{x}, \mathbf{y}) = \frac{1}{|\mathbf{x}|} \sum_{x \in \mathbf{x}} \min_{y \in \mathbf{y}} \|x - y\|_2 + \frac{1}{\|\mathbf{y}\|} \sum_{y \in \mathbf{y}} \min_{x \in \mathbf{x}} \|x - y\|_2 \tag{6}$$

The Chamfer distance is scaled by ρ , which is the length of the image diagonal, such that it is between 0 and 1. Under the setting of this problem, the reward $1 - Ch(\mathbf{x}, \mathbf{y})$ mostly falls between 0.9 and 1. In order to magnify the reward difference among actions, we exponentiated $1 - Ch(\mathbf{x}, \mathbf{y})$ to the power of 20. We add the other component to the reward function based on pixel differences in order to differentiate shapes with similar sizes and locations. The final reward function can be described as follow:

$$R(\mathbf{x}, \mathbf{y}) = \max(\delta, (1 - \frac{Ch(\mathbf{x}, \mathbf{y})}{\rho})^\gamma + \frac{\sum_{x \in \mathbf{x} \cap \mathbf{y}} 1}{\sum_{x \in \mathbf{x}} 1}) \tag{7}$$

with \mathbf{x} representing the original image and \mathbf{y} representing the generated image and $\gamma = 20$ in this setting. When a generated image receives a very low reward from the function, its exact reward

value provides little insight on its performance and is largely depending on its target image, thus we chose $\delta = 0.3$ as the minimum reward in order to simplify the reward function’s behavior when the generated images have poor qualities. Similar reward clipping idea was also proposed in DQN [Mnih *et al.*, 2013] and they used it to unify the reward ranges across different games to $[-1, 1]$.

Our setup closely follows [Sharma *et al.*, 2018]. However, naively extending [Sharma *et al.*, 2018] by optimizing reinforcement learning objectives does not learn to generate correct grammatical programs. We introduce two crucial designs to improve the learning. First, we adopt a grammar encoded tree LSTM to ensure a valid output sequence with an image stack to provide intermediate images. Second, we propose a lower-variance entropy estimator to improve both the estimation and optimization.

4.1 Grammar Encoded Tree LSTM

There are 3 main production rules in the grammatical program generation. One is shape selection (P), another type is operation selection (T), and the third type is grammar selection (E). Grammar selection in this problem setting includes $E \rightarrow EET$, and $E \rightarrow P$ as in the grammar definition which decides whether the program will expand. Let the set of shapes to be \mathcal{P} , the set of operations to be \mathcal{T} , and the set of non-terminal outcomes to be \mathcal{G} (e.g. EET in (2)). A naive parameterization is to let the candidate set of the LSTM output to be $\{S, \$\} \cup \mathcal{T} \cup \mathcal{P}$, where $\$$ is the end token, and treat it as a standard language model to generate the program [Sharma *et al.*, 2018]. The model does not explicitly encode grammar structures, and expect the model to capture it implicitly during the learning process. The drawback is that the generated program is not guaranteed to be always grammatically correct. For example, the possible generation can be $S + + + \$$, which is an invalid program.

Instead of blindly sampling terminal tokens, it is easy to sample grammatically correct programs based on its production rules given a well defined grammar. Therefore, we propose a *grammar (tree) LSTM* which takes the grammar production rule into account for generation, and it is guaranteed to always generate grammatically correct program and significantly reduce the search space during the training. Grammar encoded models have been used in language tasks, such as [Tai *et al.*, 2015; Wang *et al.*, 2018]. They used multiple RNN’s for different non-terminal tokens to ensure that the output words follow the grammar rules. Such models are not popular because there are significant amount of exceptions to the rules in natural languages. In contrast, CFG is a well-defined grammar making it an ideal candidate to be modeled by grammar encoded tree LSTM.

The proposed model can be simply understood as an RNN model with a *masking mechanism* by properly maintaining a stack to rule out invalid outputs. We increase the size of the output space from $2 + |\mathcal{P}| + |\mathcal{T}|$ of the previous approach (e.g. [Sharma *et al.*, 2018]) to $2 + |\mathcal{P}| + |\mathcal{T}| + |\mathcal{G}|$ by including the non-terminal tokens. During the generation, we maintain a stack to trace the current production rule. Based on the current non-terminal token, we use the masking mechanism to weed out the invalid output candidates. For example, if we are handling the non-terminal T , we mask the invalid output to reduce the candidate size from $2 + |\mathcal{P}| + |\mathcal{T}| + |\mathcal{G}|$ to $|\mathcal{T}|$ only. For more details, please refer to [Tai *et al.*, 2015].

To boost the performance, we further propose an image stack to maintain the intermediate images during the generation and feed them into the model to provide additional information. An example for better understanding is shown below and you can trace each step through Figure 1.

- A grammar stack with a start token S and an end token $\$$ as well as an empty image stack is initialized.
- In the first iteration, the token S is popped out. Following (1), all other options will be masked except E , the only possible output. E token is added to the stack.
- In the second iteration, or any iteration where the token E is popped, the input for all examples and all softmax outputs are masked except the entries representing EET and P according to (2). If EET is sampled, T , E and E tokens will be added to the stack separately in that exact order to expand the program further. If P is sampled, it will be added to the stack and the program cannot expand further.
- If T is popped out of the stack, the output space for that iteration will be limited to all the operations (3). Similarly, if P is popped out, the output space is limited to all the geometric shapes (4).

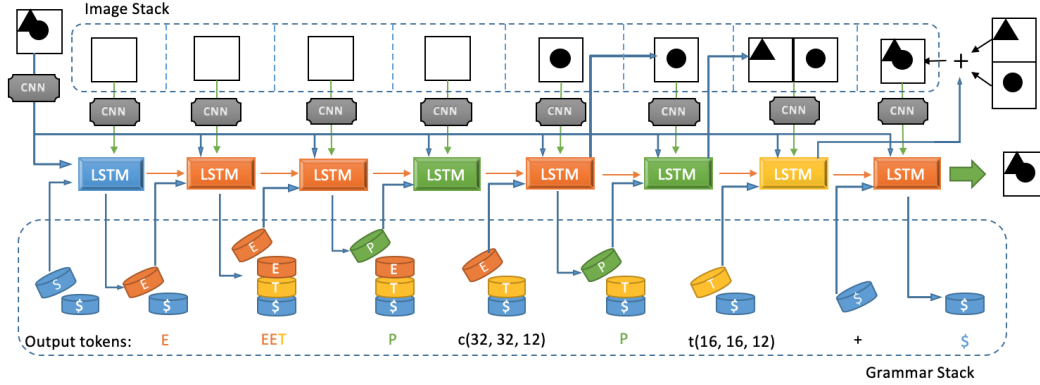


Figure 1: This is an example of grammar encoded tree LSTM at work. The top layer of canvases demonstrates the image stack and the bottom layer demonstrates the grammar stack. The blue, orange, yellow and green colored LSTM cell generates grammatical symbols according to the CFG rule (1), (2), (3) and (4) respectively. In implementation, we can constrain the output space by adding a mask to the output of the LSTM and render the invalid options with close to zero probability of being sampled.

- When a shape token is sampled, it will not be added to the grammar stack as they do not contribute to the program structure. Instead, the image of the shape will be pushed onto the corresponding image stack.
- When an operation token is sampled, it also will not be added to the grammar stack. Instead, we pop out the top two images to apply the operation on them and push the final image onto the image stack again.
- When the stack has popped out all the added tokens, the end token \$ will be popped out in the last iteration. We then finish the sampling as standard RNN language models.

Before finishing generating a program, there can be multiple images present yet to be assembled by operations in the image stack. We consider them to be the observations in the process and utilize LSTM with those observations as a part of the input to better infer our future direction in the search space.

In this process, the model will produce a sequence of tokens, including grammatical, shape and operation tokens. We only keep all the terminal tokens as the final output program and discard the rest. The programs are ensured to be grammatically correct.

In practice, we implement the masking mechanism by adding a vector to the output before passing into softmax layer to get the probability. The vector contains 0 for valid output and large negative numbers for invalid ones. This makes sure that invalid options will have almost zero probability of being sampled. The input of the RNN cell includes encoded target image and intermediate images from the image stack, embedded pop-out token from grammar stack and the hidden state from the RNN's last iteration. Following previous works in NLP, we call the model *Tree LSTM*. The exact algorithm is in Algorithm 1.

4.2 Exploration with Entropy Regularization

Entropy regularization in reinforcement learning is a standard practice for encouraging exploration. We argue that a careful design of entropy estimation with lower variance can enhance the exploration effect.

Algorithm 1 Tree LSTM Model

Input: Grammar Stack S , Image Stack I , Target Image \mathbf{x} , Sample Set \mathbb{B}

```

1: function TREELSTM( $S, I, \mathbb{B}, \mathbf{x}$ )
2:    $\tilde{\mathbf{x}} \leftarrow \text{ENCODE}(\mathbf{x})$ 
3:   for  $(s^i, \phi_{i,j}, G_{\phi_{i,j}}) \in \mathbb{B}$  do
4:      $g_i \leftarrow S_i.\text{POP}()$ 
5:      $\tilde{g}_i \leftarrow \text{EMBED}(g_i)$ 
6:      $\tilde{I}_i \leftarrow \text{ENCODE}(I_i)$ 
7:      $H_{i,j} \leftarrow \text{LSTM}(\tilde{g}_i, \tilde{I}_i, \tilde{\mathbf{x}}, H_{i,j-1})$ 
8:      $\mathbf{p}_{i,j} \leftarrow \text{SOFTMAX}(f(H_{i,j}) + \text{MASK}(g_i))$ 
9:     Estimate entropy at this node  $v_{i,j}$ :
10:     $\mathcal{H}(v_{i,j}) = \mathbf{p}_{i,j} \cdot \log \mathbf{p}_{i,j}$ 
11:    Update the log probabilities of partial sequences
12:     $\phi_{i,j} = \mathbf{1} \cdot \phi_{i,j-1} + \log \mathbf{p}_{i,j}$ 
13:  end for
14:  return  $\phi_{:,j+1}, \mathcal{H}(v_{i,j})$ 
15: end function

```

Let S to be the random variable of possible programs. The entropy is denoted as $\mathcal{H}(S) = \mathbb{E}[-\log P(S)]$ ¹. The possible outcomes of S can be exponentially large. Therefore, we usually estimate the entropy via

$$\hat{\mathcal{H}} = -\frac{1}{K} \sum_{i=1}^K \log P(s^i). \quad (8)$$

with finite samples $\{s^i\}_{i=1}^K$. Without further assumption, we are not able to improve $\hat{\mathcal{H}}$. However, we can decompose program into $S = X_1 \dots X_n$, where each X_j is the random variable for the token at position j in the program. Under autoregressive models (e.g. RNN), we can further access the conditional probability. Therefore, we propose a decomposed entropy estimator $\hat{\mathcal{H}}_D$ as

$$\hat{\mathcal{H}}_D = \frac{1}{K} \sum_{i=1}^K \sum_{j=1}^n \mathcal{H}(X_j | X_1 = x_1^i, \dots, X_{j-1} = x_{j-1}^i), \quad (9)$$

where $s^i = x_1^i, \dots, x_n^i$, and $\mathcal{H}(X_j | X_1 = x_1^i, \dots, X_{j-1} = x_{j-1}^i)$ is the conditional entropy.

Lemma 4.1. *The proposed decomposed entropy estimator $\hat{\mathcal{H}}_D$ is unbiased with lower variance, that is $\mathbb{E}[\hat{\mathcal{H}}_D] = \mathcal{H}(S)$ and $\text{Var}(\hat{\mathcal{H}}_D) \leq \text{Var}(\hat{\mathcal{H}})$.*

The proof is simple by following [Cover and Thomas, 2012] and we leave it in Appendix B and C.

4.3 Effective Entropy Optimization

We have established our REINFORCE with entropy regularization objective and the next step is to optimize it in an efficient way. In this section, we will show that sampling without replacement is more data-efficient than sampling with replacement. We demonstrate our point by an experiment in a synthetic setting (Figure 2). In this experiment, we initialize a distribution of 100 variables with three of them having significantly higher probability than the others (as in the second image in Figure 2). The loss function is the estimated entropy from the sampled variables. For sampling with replacement, the estimation is $\frac{1}{m} \sum_{i=1}^m \log p_i$. For sampling without replacement, the estimation is $\sum_{i=1}^m \frac{p_i}{q_i} \log p_i$. In both cases, p_i represents the probability of the i -th sampled variable and m is the total variables drawn. q_i represents the re-normalized probability of the variable after removing the previously sampled variables. $\frac{p_i}{q_i}$ is the importance weighting for each term.

¹Here we overload S and P as used in (1) and (2) to follow the convention.

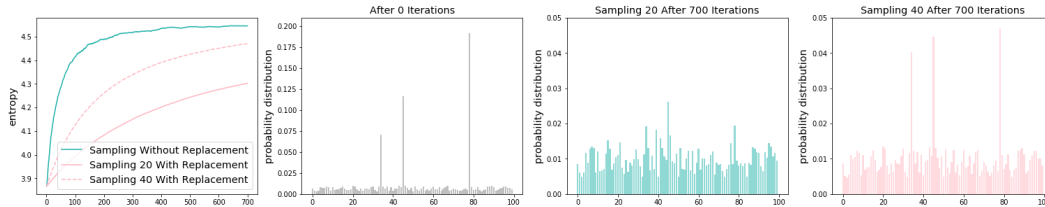


Figure 2: The left most image demonstrates the entropy value increases over 700 iterations by sampling 20 distinct samples with and without replacement as well as sampling 40 samples with replacement. The second image shows the initial distribution. The third and fourth images show the ending distributions after we maximize the entropy by sampling with and without replacement.

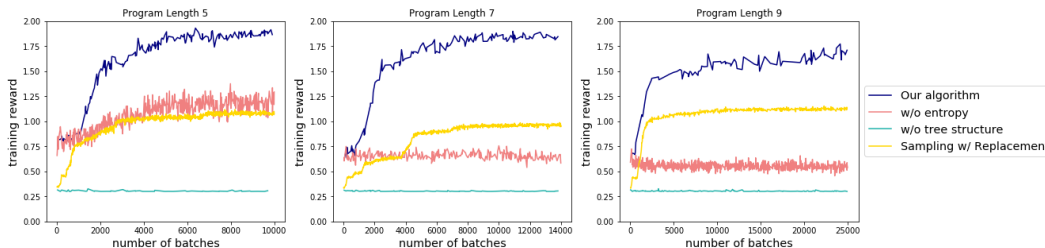


Figure 3: From left to right, we have reward per batch for programs of length 5, 7 and 9. It demonstrates the performance of our algorithm and controlled comparison in performance with removing one component at a time.

In this experiment, we chose $m = 20$ for sampling without replacement and $m = 20, 40$ for sampling with replacement. The increase in entropy with sampling 20 variables without replacement is more rapid than sampling 40 variables with replacement under the same setting. At the end of the 700 iterations, the distribution of sampling without replacement is visibly more uniform than the distribution from sampling with replacement.

Implementing sampling without replacement on a tree structure in this case can be challenging. We do not have the resources to instantiate every possible path and perform sampling without replacement bottom-up. Instead, we adopt a form of stochastic beam search by combining top-down sampling without replacement with Gumbel trick that is equivalent to sampling without replacement bottom-up [Kool *et al.*, 2019b]. Please refer to Algorithm 2 for the full algorithm including the sampling without replacement and tree LSTM components and Appendix A for more details.

5 Experiments

In the experiment section, we are going to investigate how much each of the design features affect the learning process. We will show that the entropy estimator we proposed earlier (9) has smaller variance than the sequence log probability method (8). We also train the model with supervision and report its result in comparison to the unsupervised method. For the last experiment, we compare the data-efficiency of sampling with and without replacement.

5.1 Reward Comparison of Design Features

We used synthetic dataset to test our algorithm and compare the effects of each feature. The algorithm chooses from 27 shape actions, 3 operation actions and 2 grammar actions to create image on a 64 by 64 canvas. The 27 shape actions have their size, position in the canvas as well as the type of geometry (circle, triangle or square) encoded in the selection. For evaluation purpose, our synthetic dataset has the ground truth program to each of the images. We separated our dataset by the length of the program to study the image complexity’s effect on the learning process. Program length also implies the number of shapes in the images. Programs of length 5 have 3 shapes and 2 operation actions and

Algorithm 2 Sampling w/o Replacement Tree LSTM

Input: Target Image \mathbf{x} , Number of beams k **Initialize:** Grammar stack S , Image stack I , Beam set \mathbb{B}

Encode the target image $\tilde{T} \leftarrow \text{ENCODE}(T)$
 $\mathbb{B} = \{s^i | s^i = \emptyset, \phi_{i,0} = 0, G_{\phi_{i,0}} = 0\}$
 $\mathcal{H}(v) = 0$
for $j := 1$ to n **do**
 $\phi_{:,j}, \mathcal{H}(v_{i,j}) \leftarrow \text{TREELSTM}(S, I, \mathbb{B}, \mathbf{x})$
 $\mathbb{B} \leftarrow \text{SAMPLE_WITHOUT_REPLACEMENT}(\phi_{:,j}, \mathbb{B}, k)$ (See [Kool *et al.*, 2019b])
 $\mathcal{H}(v) \leftarrow \mathcal{H}(v) + \frac{1}{W_j(S)} \sum_j \frac{p_{\theta}(s_j^i)}{q_{\theta, \kappa}(s_j^i)} \mathcal{H}(v_{i,j})$ (Entropy estimation by (9) and Appendix A)
 if $s_{j+1}^i \in E$ **then** $S_i.\text{PUSH}(s_{j+1}^i)$ **else** $I_i.\text{PUSH}(s_{j+1}^i), \forall s^i \in \mathbb{B}$
end for
 $\mathbf{y}_i = \text{RENDER}(s^i)$ for $i \in 1, 2, \dots, k$
 $r_i = R(\mathbf{x}, \mathbf{y}_i)$ for $i \in 1, 2, \dots, k$
Maximize $\mathbb{E}[R(\mathbf{x}, \mathbf{y})] + \alpha \mathcal{H}(v)$

Type	Length 5	Length 7	Length 9
Training set size	3600	4800	12000
Testing set size	586	789	4630

Table 1: Dataset statistics of different program lengths.

programs of length 7 have 4 shapes and 3 operation actions etc. For each length of program, We generated all possible combinations of shape actions and operation actions in text and then filter out the duplicates and empty images. Images are considered duplicates if only 120 pixels are different between the two and are considered empty if there are no more than 120 pixels on the canvas. For dataset size information, please refer to the Table 1.

For this dataset, we sampled 19 distinct programs for each target image to approximate the objective functions. The coefficient for negative entropy is 0.05 and the learning rate is 0.01.

We compared each feature’ effects on the learning process of all three datasets with increasing difficulty. When we train the model via sampling with replacement, the training process is not able to get out of a discrete local optimum as seen in Figure 3 (yellow). The starting reward is also lower comparing to sampling without replacement because the final reward is the maximum reward of all distinct programs sampled. When we take out the entropy term in the objective function, the reward function is still able to improve with the length 5 dataset but it is barely improving with increasing program length. Without the tree structure, the reward stays around 0.3 which is the lowest possible reward in Figure 3 (green) because the program is unable to generate a valid program to render. All these design features are crucial to learning increasingly complex images. We measure our converged algorithm’s performance on the test sets of the three datasets with Chamfer and IoU metrics (Table 2 (Left)). Figure 7 provides some qualitative examples on the algorithms in Figure 3.

The Chamfer metric is defined as $(1 - \frac{Ch(\mathbf{x}, \mathbf{y})}{\rho})^\gamma$ where $\gamma = 20$ and ρ is the number of pixels on the diagonal of an image, \mathbf{x} and \mathbf{y} are the target and generated images, as defined in the first term of Equation 7. The value is between 0 and 1. If the generated image is a perfect match with the target, it will receive 1 in this metric. The IoU metric is defined as the intersection between the two images over the union: $\frac{\sum_{x \in \mathbf{x} \cap \mathbf{y}} 1}{\sum_{x \in \mathbf{x} \cup \mathbf{y}} 1}$.

5.2 Reward Comparison with Supervised Learning Method

In order to study the difference between the supervised and unsupervised learning methods, we compared the training and testing results using a supervised learning method with the same neural network model. The input at each step is the concatenation of the embedded ground truth program as well as the encoded final and intermediate images. We used the same synthetic data set and the same

Metric	Length 5	Length 7	Length 9	Chamfer	length 5	length 7	length 9
Chamfer	0.985	0.960	0.969	Training	0.997	0.996	0.994
IoU	0.996	0.964	0.969	Testing	0.987	0.906	0.833

Table 2: (Left) The performance of the converged model on the test set measured with Chamfer distance to the power of 20 and IoU. (Right) Supervised training results.

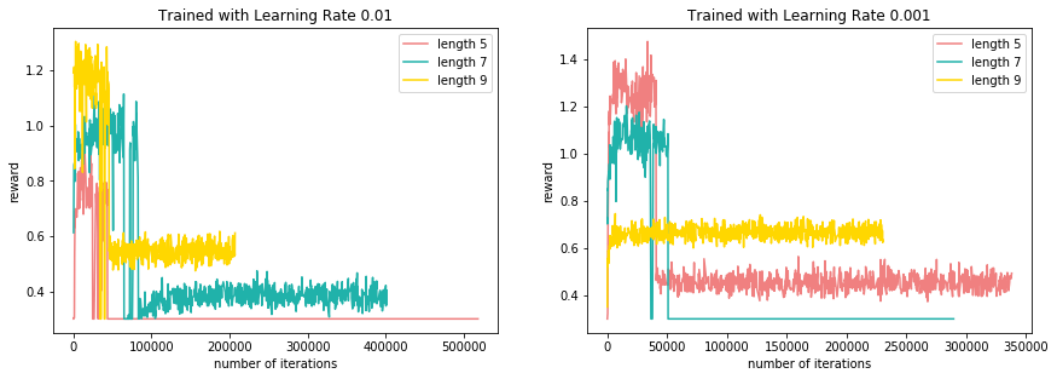


Figure 4: REINFORCE training with supervised pretraining model.

Chamfer similarity metric as in Table 2 to measure the quality of the generated data. The testing results of the supervised method worsens with the increasing complexity (program length) of the test set while the training results are almost perfect across all three datasets. Meanwhile, the unsupervised method receives consistently high scores. This shows that the supervised training method does not generalize well to unseen data in comparison to the unsupervised learning method (Table 2). Our conjecture for this result is that because the supervised learning optimizes over the loss function in the program space while the unsupervised learning optimizes over the reward function in the image space, two programs that are very close in the program space may result in very different image. We will leave the more vigorous explanation as future work.

5.3 Reward Comparison with Supervised Pretraining Method

In this experiment we pretrained the supervised model described in Section 5.2 on a third of the synthetic training dataset till convergence. We take the model and further train it with REINFORCE without the tree structure or sampling without replacement on the full training sets. We report the reward curve throughout the training process as in Figure 4. In this figure, there is a sharp drop in reward during the training process with all three datasets. Our explanation is that while the supervised pretrained model provides a grammatical structure on the output programs, it is not able to retain the structure after updates resulting in the drop in reward.

5.4 Variance Study of Entropy Estimation

In this study (Figure 5) we want to demonstrate that estimator $\hat{\mathcal{H}}_D$ achieves a lower variance than $\hat{\mathcal{H}}$ as discussed in Section 4.2.

We take a single model saved at epoch 40 during the training time of the length 5, 7, and 9 dataset and estimate the entropy with weighted sum stepwise method (Equation 9) and sequence log probability method (Equation 8). We also considered two sampling schemes: sampling without replacement and sampling with replacement. We combine both entropy estimation methods with the two sampling schemes creating four instances for comparisons. The x-axis of the plot documents the number of distinct programs in the sampling without replacement method. The number of distinct programs is replaced with the number of repetitions for sampling with replacement. We obtain a single estimation of the entropy by taking the mean after running the sampling with replacement scheme the same

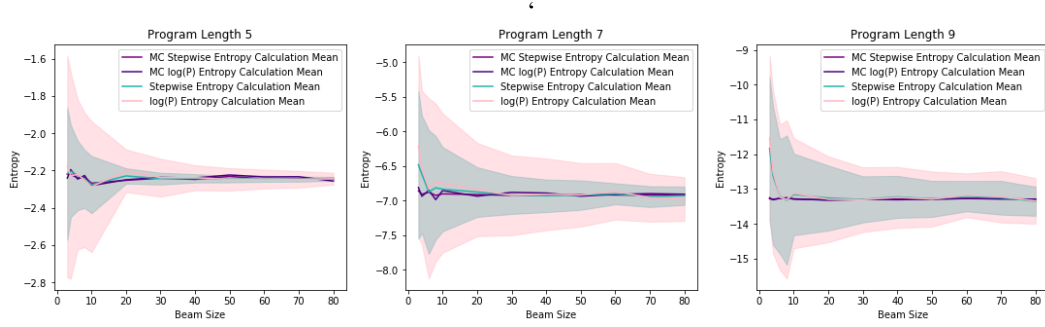


Figure 5: Compare the estimation of the entropy following the Equation 11 as a weighted sum of stepwise entropy vs. taking the average of the log probability of the sequence. The beam size goes from 2 to 80. From left to right, we demonstrate the result on datasets of three program lengths.

number of times as the number of distinct programs. We further repeat the estimation 100 times to obtain the mean and variance. The means of sampling with replacement method act as a baseline for the means of the sampling without replacement method while we compare the variances of the two entropy estimation methods.

We experimented on the number of distinct programs from 2 to 80. In all three datasets, the stepwise entropy estimator (green) shows significantly smaller variance. But we notice that longer programs, or more complex images, require much more distinct programs to reduce the variance in estimation. This makes sense because the search space increases exponentially with longer program length. There also exists bias in the estimation using the sampling without replacement method. In all three cases, the bias resolves after the number of distinct programs increase to be greater than 10. The bias is greater in dataset with longer program length.

6 Discussion

In this paper, we proposed an entropy regularized REINFORCE based algorithm with grammar encoded tree LSTM that leverage grammatical structures to parse a CSG image into context-free grammar. It is the first paper to successfully parse a CSG image with non-differentiable renderer into CFG without program supervision. Our ingredients include a tree LSTM that guarantees the output programs' correctness, an unbiased and low-variance entropy estimator of a program sequence, and sampling without replacement to improve data and optimization efficiency. Our experiments have demonstrated the importance of each of our design features quantitatively and qualitatively.

References

- Martin Arjovsky, Soumith Chintala, and Léon Bottou. Wasserstein gan. *arXiv preprint arXiv:1701.07875*, 2017.
- Matej Balog, Alexander L. Gaunt, Marc Brockschmidt, Sebastian Nowozin, and Daniel Tarlow. Deepcoder: Learning to write programs. In *International Conference on Representation Learning (ICLR)*, 2017.
- Xi Chen, Yan Duan, Rein Houthoofd, John Schulman, Ilya Sutskever, and Pieter Abbeel. Infogan: Interpretable representation learning by information maximizing generative adversarial nets. In *Advances in neural information processing systems*, 2016.
- Thomas M Cover and Joy A Thomas. *Elements of information theory*. John Wiley & Sons, 2012.
- Jacob Devlin, Jonathan Uesato, Surya Bhupatiraju, Rishabh Singh, Abdel-rahman Mohamed, and Pushmeet Kohli. Robustfill: Neural program learning under noisy i/o. In *Proceedings of the 34th International Conference on Machine Learning-Volume 70*, pages 990–998. JMLR. org, 2017.
- Kevin Ellis, Daniel Ritchie, Armando Solar-Lezama, and Josh Tenenbaum. Learning to infer graphics programs from hand-drawn images. In *Advances in neural information processing systems*, pages 6059–6068, 2018.
- Kevin Ellis, Maxwell Nye, Yewen Pu, Felix Sosa, Josh Tenenbaum, and Armando Solar-Lezama. Write, execute, assess: Program synthesis with a repl, 2019.
- Yaroslav Ganin, Tejas Kulkarni, Igor Babuschkin, SM Eslami, and Oriol Vinyals. Synthesizing programs for images using reinforced adversarial learning. *arXiv preprint arXiv:1804.01118*, 2018.
- Ian Goodfellow, Jean Pouget-Abadie, Mehdi Mirza, Bing Xu, David Warde-Farley, Sherjil Ozair, Aaron Courville, and Yoshua Bengio. Generative adversarial nets. In *Advances in neural information processing systems*, pages 2672–2680, 2014.
- David Ha and Douglas Eck. A Neural Representation of Sketch Drawings. *ArXiv e-prints*, April 2017.
- Irina Higgins, Loic Matthey, Arka Pal, Christopher Burgess, Xavier Glorot, Matthew Botvinick, Shakir Mohamed, and Alexander Lerchner. beta-vae: Learning basic visual concepts with a constrained variational framework. *ICLR*, 2017.
- Zhewei Huang, Wen Heng, and Shuchang Zhou. Learning to paint with model-based deep reinforcement learning. *arXiv preprint arXiv:1903.04411*, 2019.
- Philip M Hubbard. *Constructive solid geometry for triangulated polyhedra*. 1990.
- Hyunjik Kim and Andriy Mnih. Disentangling by factorising. *arXiv preprint arXiv:1802.05983*, 2018.
- Diederik P Kingma and Max Welling. Auto-encoding variational bayes. *arXiv preprint arXiv:1312.6114*, 2013.
- Wouter Kool, Herke van Hoof, and Max Welling. Buy 4 reinforce samples, get a baseline for free! 2019.
- Wouter Kool, Herke Van Hoof, and Max Welling. Stochastic beams and where to find them: The gumbel-top-k trick for sampling sequences without replacement. In *International Conference on Machine Learning*, pages 3499–3508, 2019.
- Chun-Liang Li, Wei-Cheng Chang, Yu Cheng, Yiming Yang, and Barnabás Póczos. Mmd gan: Towards deeper understanding of moment matching network. In *Advances in Neural Information Processing Systems*, pages 2203–2213, 2017.
- Tzu-Mao Li, Miika Aittala, Frédo Durand, and Jaakko Lehtinen. Differentiable monte carlo ray tracing through edge sampling. In *SIGGRAPH Asia 2018 Technical Papers*, page 222. ACM, 2018.
- Yunchao Liu, Zheng Wu, Daniel Ritchie, William T Freeman, Joshua B Tenenbaum, and Jiajun Wu. Learning to describe scenes with programs. 2018.
- Hsueh-Ti Derek Liu, Michael Tao, Chun-Liang Li, Derek Nowrouzezahrai, and Alec Jacobson. Beyond pixel norm-balls: Parametric adversaries using an analytically differentiable renderer. 2019.

- Francesco Locatello, Stefan Bauer, Mario Lucic, Gunnar Rätsch, Sylvain Gelly, Bernhard Schölkopf, and Olivier Bachem. Challenging common assumptions in the unsupervised learning of disentangled representations. *arXiv preprint arXiv:1811.12359*, 2018.
- Volodymyr Mnih, Koray Kavukcuoglu, David Silver, Alex Graves, Ioannis Antonoglou, Daan Wierstra, and Martin Riedmiller. Playing atari with deep reinforcement learning. *arXiv preprint arXiv:1312.5602*, 2013.
- Aaron van den Oord, Nal Kalchbrenner, and Koray Kavukcuoglu. Pixel recurrent neural networks. *arXiv preprint arXiv:1601.06759*, 2016.
- Lukasz Romaszko, Christopher KI Williams, Pol Moreno, and Pushmeet Kohli. Vision-as-inverse-graphics: Obtaining a rich 3d explanation of a scene from a single image. In *Proceedings of the IEEE International Conference on Computer Vision*, pages 851–859, 2017.
- Gopal Sharma, Rishabh Goyal, Difan Liu, Evangelos Kalogerakis, and Subhansu Maji. Csgnet: Neural shape parser for constructive solid geometry. In *Proceedings of the IEEE Conference on Computer Vision and Pattern Recognition*, pages 5515–5523, 2018.
- Richard Shin, Illia Polosukhin, and Dawn Song. Improving neural program synthesis with inferred execution traces. In *Advances in Neural Information Processing Systems*, pages 8917–8926, 2018.
- Kai Sheng Tai, Richard Socher, and Christopher D Manning. Improved semantic representations from tree-structured long short-term memory networks. In *Proceedings of the 53rd Annual Meeting of the Association for Computational Linguistics and the 7th International Joint Conference on Natural Language Processing (Volume 1: Long Papers)*, pages 1556–1566, 2015.
- Yonglong Tian, Andrew Luo, Xingyuan Sun, Kevin Ellis, William T Freeman, Joshua B Tenenbaum, and Jiajun Wu. Learning to infer and execute 3d shape programs. *arXiv preprint arXiv:1901.02875*, 2019.
- Shubham Tulsiani, Hao Su, Leonidas J Guibas, Alexei A Efros, and Jitendra Malik. Learning shape abstractions by assembling volumetric primitives. In *Proceedings of the IEEE Conference on Computer Vision and Pattern Recognition*, pages 2635–2643, 2017.
- Aaron van den Oord, Oriol Vinyals, et al. Neural discrete representation learning. In *Advances in Neural Information Processing Systems*, pages 6306–6315, 2017.
- Xinyi Wang, Hieu Pham, Pengcheng Yin, and Graham Neubig. A tree-based decoder for neural machine translation. *arXiv preprint arXiv:1808.09374*, 2018.
- Ronald J Williams. Simple statistical gradient-following algorithms for connectionist reinforcement learning. *Machine learning*, 8(3-4):229–256, 1992.
- Jiajun Wu, Joshua B Tenenbaum, and Pushmeet Kohli. Neural scene de-rendering. In *Proceedings of the IEEE Conference on Computer Vision and Pattern Recognition*, pages 699–707, 2017.
- Shunyu Yao, Tzu Ming Hsu, Jun-Yan Zhu, Jiajun Wu, Antonio Torralba, Bill Freeman, and Josh Tenenbaum. 3d-aware scene manipulation via inverse graphics. In *Advances in Neural Information Processing Systems*, pages 1887–1898, 2018.
- Amit Zohar and Lior Wolf. Automatic program synthesis of long programs with a learned garbage collector. In *Advances in Neural Information Processing Systems*, pages 2094–2103, 2018.

A Sampling Without Replacement

This section describes how we achieve sampling without replacement with the help of stochastic beam search [Kool *et al.*, 2019b].

At each step of generation, the algorithm chooses the top k branches to expand based on the $G_{\phi_{i,j}}$ score at time step j . The $G_{\phi_{i,j}}$ score is sampled from $\text{Gumble}(\phi_{i,j})$, where $\phi_{i,j}$ is the log probability of the partial sequence i at time step j , conditioned on its parent’s $G_{\phi_{i,j-1}}$ score being the maximum. Please refer to A for details in the branching process.

The sampling without replacement algorithm requires correct scaling of the objective functions to ensure unbiasedness. The scaling term is $\frac{p_{\theta}(s^i)}{q_{\theta,\kappa}(s^i)}$. $p_{\theta}(s^i)$ represents the probability of the sequence s^i and S represents the set of all sampled sequences s^i for $i = 1, 2, \dots, K$. $q_{\theta,\kappa}(s_j^i) = P(G_{s_j^i} > \kappa)$

where κ is the $(k + 1)$ -th largest $G_{\phi_{i,j}}$ score among all the possible branches. It acts as a threshold for branching selection. During implementation, we need to keep an extra beam, thus $k + 1$ beams in total, to accurately estimate κ in order to ensure the unbiasedness of the estimator without normalization. Additional normalization terms $W^i(S) = W(S) - \frac{p_\theta(s^i)}{q_{\theta,\kappa}(s^i)} + p_\theta(s^i)$ and $W(S) = \sum_{s^i \in S} \frac{p_\theta(s^i)}{q_{\theta,\kappa}(s^i)}$ are employed to reduce variance but they increase bias in the final estimation. The exact objective is as follows [Kool *et al.*, 2019a]:

$$\nabla_{\theta} \mathbb{E}_{s \sim p_{\theta}(s)} [f(s)] \approx \sum_{s^i \in S} \frac{1}{W^i(S)} \cdot \frac{\nabla_{\theta} p_{\theta}(s^i)}{q_{\theta,\kappa}(s^i)} \left(f(s^i) - \frac{B(S)}{W(S)} \right) \quad (10)$$

The baseline term is defined as $B(S) = \sum_{s^i \in S} \frac{p_{\theta}(s^i)}{q_{\theta,\kappa}(s^i)} f(s^i)$. Incorporating a baseline into the REINFORCE objective is a standard practice in order to reduce variance in the estimation.

Entropy estimation uses a similar scaling scheme as the REINFORCE objective:

$$\mathcal{H}(X_1, X_2, X_3, \dots, X_n) \approx \sum_{j=1}^n \frac{1}{W_j(S)} \sum_{s^i \in S} \frac{p_{\theta}(s_j^i)}{q_{\theta,\kappa}(s_j^i)} \mathcal{H}(X_j | X_1 = x_1^i, \dots, X_{j-1} = x_{j-1}^i)$$

where $W_j(S) = \sum_{s^i \in S} \frac{p_{\theta}(s_j^i)}{q_{\theta,\kappa}(s_j^i)}$ and s_j^i denotes the first j elements of the sequence s^i . The estimator is unbiased excluding the $\frac{1}{W_j(S)}$ term. The normalization term reduces the variance of the estimator.

The input of the function SAMPLING_WITHOUT_REPLACEMENT at time step j is a matrix $\phi_{:,j+1}$. Each row of the matrix represents the $k + 1$ beams that we maintain and the column of the matrix is the size of the action space. The entry (i, h) in the matrix is equal to $\phi_{i,j} + \log P(X_{j+1} = h | X_1 = x_1^i, \dots, X_j = x_j^i)$ where s_j^i consists of $x_1^i, x_2^i, \dots, x_j^i$. Row i of the matrix represents the log probability of the partial sequence i expanding one more step with all potential actions.

For each beam, we sample a Gumbel random variable with location at each of the element of the vector $\phi_{i,j+1}$. Then we need to adjust the Gumbel random variable by conditioning on its parent's stochastic score being the largest, the resulting value is the stochastic score for each of the potential expansions.

$$\tilde{\mathbf{G}}_{\phi_{i,j+1}} = -\log(\exp(-\mathbf{1} \cdot G_{\phi_{i,j}})) - \exp(-\mathbf{1} \cdot Z_{i,j+1}) + \exp(-\mathbf{G}_{\phi_{i,j+1}})$$

Here $Z_{i,j+1}$ is the largest value in the vector $\mathbf{G}_{\phi_{i,j+1}}$ and $G_{\phi_{i,j}}$ is the stochastic score of the parent of i -th beam's all the possible outcomes at step $j + 1$. Conditioning on the parent stochastic score being the largest in this top-down sampling scheme makes sure that each leaf's stochastic score $G_{\phi_{i,j}} \sim \text{Gumbel}(\phi_{i,j})$ independently, equivalent to sampling the sequences bottom up [Kool *et al.*, 2019b]. Once we have aggregated all the stochastic scores for all potential expansions of $k + 1$ beams, we select the top $k + 1$ expansions. Note that the reason that we maintain one more beam than we intended to expand because we need the $k + 1$ largest stochastic score to be the threshold during estimation of the entropy and REINFORCE objective.

B Proof of Stepwise Entropy Estimation's Unbiasness

Entropy of a sequence can be decomposed into the sum of the conditional entropy at each step conditioned on the previous values. This is also called the chain rule for entropy calculation. Let X_1, X_2, \dots, X_n be drawn from $P(X_1, X_2, \dots, X_n)$ [Cover and Thomas, 2012]:

$$\mathcal{H}(X_1, X_2, \dots, X_n) = \sum_{j=1}^n \mathcal{H}(X_j | X_1, \dots, X_{j-1}) \quad (11)$$

Algorithm 3 Sampling w/o Replacement

Input: Log probability of sequences up to time step j $\phi_{:,j}$, Beam Set \mathbb{B} , Number of beams k

```
1: function SAMPLING_WITHOUT_REPLACEMENT( $\phi_{:,j}, \mathbb{B}, k$ )
2:    $\tilde{G} \leftarrow \emptyset$ 
3:   for  $s^i \in \mathbb{B}$  do
4:      $G_{\phi_{i,j}} \sim \text{Gumbel}(\phi_{i,j})$ 
5:      $Z_{i,j} \leftarrow \max(G_{\phi_{i,j}})$ 
6:      $\tilde{G}_{\phi_{i,j}} \leftarrow -\log(\exp(-\mathbf{1} \cdot G_{\phi_{i,j-1}})) - \exp(-\mathbf{1} \cdot Z_{i,j}) + \exp(-G_{\phi_{i,j}})$ 
7:     Aggregate the values in the vector  $\tilde{G}_{\phi_{i,j}}$ 
8:      $\tilde{G} \leftarrow \tilde{G} \cup \tilde{G}_{\phi_{i,j}}$ 
9:   end for
10:  Choose top  $k + 1$  values in  $\tilde{G}$ 
11:   $\mathbb{B} = \{s^{\tilde{i}} | s^{\tilde{i}} \cup s_j^{\tilde{i}}, \phi_{i,j}, G_{\phi_{i,j}} = \tilde{G}_{\phi_{i,j}}\}$ 
12:  where  $\tilde{i} \in k + 1$ 
13:  return  $\mathbb{B}$ 
14: end function
```

If we sum up the empirical entropy at each step after the softmax output, we can obtain an unbiased estimator of the entropy. Let S be the set of sequences that we sampled and each sampled sequence s^i consists of X_1, X_2, \dots, X_n :

$$\begin{aligned} & \mathbb{E}_{X_1, X_2, \dots, X_{j-1}}(\hat{\mathcal{H}}_D) \\ &= \mathbb{E}_{X_1, X_2, \dots, X_{j-1}}\left(\frac{1}{|S|} \sum_{i \in |S|} \sum_{j=1}^n \mathcal{H}(X_j | X_1 = x_1^i, \dots, X_{j-1} = x_{j-1}^i)\right) \\ &= \frac{1}{|S|} \cdot |S| \sum_{j=1}^n \mathcal{H}(X_j | X_1, \dots, X_{j-1}) \\ &= \mathcal{H}(X_1, X_2, \dots, X_n) \end{aligned}$$

In order to incorporate the stepwise estimation of the entropy into the beam search, we use the similar reweighting scheme as the REINFORCE objective. The difference is that the REINFORCE objective is reweighted after obtaining the full sequence because we only receive the reward at the end and here we reweight the entropy at each step. We denote each time step by j and each sequence by i , the set of sequences selected at time step j is S_j and the complete set of all possible sequences of length j is T_j and $S_j \in T_j$. We are taking the expectation of the estimator over the $G_{\phi_{i,j}}$ scores. As we discussed before, at each step, each potential beam receives a stochastic score $G_{\phi_{i,j}}$. The beams associated with the top- $k + 1$ stochastic scores are chosen to be expanded further and κ is the $k + 1$ -th largest $G_{\phi_{i,j}}$. κ can also be seen as a threshold in the branching selection process and $q_{\theta, \kappa}(s_j^i) = P(G_{s_j^i} > \kappa) = 1 - \exp(-\exp(\phi_{i,j} - \kappa))$. For details on the numerical stable implementation of $q_{\theta, \kappa}(s_j^i)$, please refer to [Kool *et al.*, 2019b].

$$\begin{aligned} & \mathbb{E}_{G_\phi} \left(\sum_{j=1}^n \sum_{s_j^i \in S_j} \frac{p_\theta(s_j^i)}{q_{\theta, \kappa}(s_j^i)} \mathcal{H}(X_j | X_1 = x_1^i, X_2 = x_2^i, \dots, X_{j-1} = x_{j-1}^i) \right) \\ &= \sum_{j=1}^n \mathbb{E}_{G_\phi} \left(\sum_{i \in |T_j|} \frac{p_\theta(s_j^i)}{q_{\theta, \kappa}(s_j^i)} \mathcal{H}(X_j | X_1 = x_1^i, X_2 = x_2^i, \dots, X_{j-1} = x_{j-1}^i) \mathbb{1}_{\{x_1^i, \dots, x_j^i\} \in S_j} \right) \\ &= \sum_{j=1}^n \sum_{i \in |T_j|} p_\theta(s_j^i) \mathcal{H}(X_j | X_1 = x_1^i, X_2 = x_2^i, \dots, X_{j-1} = x_{j-1}^i) \mathbb{E}_{G_\phi} \left(\frac{\mathbb{1}_{\{s_j^i = x_1^i, \dots, x_j^i\} \in S_j}}{q_{\theta, \kappa}(s_j^i)} \right) \end{aligned}$$

$$\begin{aligned}
&= \sum_{j=1}^n \mathcal{H}(X_j | X_1, X_2, \dots, X_{j-1}) \cdot 1 \\
&= \mathcal{H}(X_1, X_2, \dots, X_n)
\end{aligned}$$

For the proof of $\mathbb{E}_{G_\phi} \left(\frac{\mathbb{1}_{\{s_j^i \in S_j\}}}{q_{\theta, \kappa}(s_j^i)} \right) = 1$, please refer to the paper [Kool *et al.*, 2019b], appendix D.

C Proof of Lower Variance of the Stepwise Entropy Estimator

We will continue using the notations from above. We want to compare the variance of the two entropy estimator $\hat{\mathcal{H}}$ and the stepwise entropy estimator $\hat{\mathcal{H}}_D$ and show that the second estimator has lower variance.

Proof. We abuse \mathbb{E}_{X_j} to be $\mathbb{E}_{X_j | X_1, \dots, X_{j-1}}$ and Var_{X_j} to be $\text{Var}_{X_j | X_1, \dots, X_{j-1}}$ to simplify the notations.

$$\begin{aligned}
&\text{Var}_{X_1, X_2, \dots, X_n} \left(\frac{1}{|S|} \sum_{i \in |S|} \sum_{j=1}^n \mathcal{H}(X_j | X_1 = x_1^i, \dots, X_{j-1} = x_{j-1}^i) \right) \\
&= \frac{1}{|S|^2} \sum_{i \in |S|} \sum_{j=1}^n \text{Var}_{X_1, X_2, \dots, X_n} (\mathcal{H}(X_j | X_1 = x_1^i, \dots, X_{j-1} = x_{j-1}^i)) \\
&= \frac{1}{|S|^2} \sum_{i \in |S|} \sum_{j=1}^n (\mathbb{E}(\mathcal{H}^2(X_j | X_1 = x_1^i, \dots, X_{j-1} = x_{j-1}^i)) - \\
&\quad \mathbb{E}^2(\mathcal{H}(X_j | X_1 = x_1^i, \dots, X_{j-1} = x_{j-1}^i))) \\
&= \frac{1}{|S|^2} \sum_{i \in |S|} \sum_{j=1}^n (\mathbb{E}_{X_1, \dots, X_{j-1}} \mathbb{E}_{X_j}^2 (\log P(X_j | X_1 = x_1^i, \dots, X_{j-1} = x_{j-1}^i)) - \\
&\quad \mathbb{E}_{X_1, \dots, X_{j-1}}^2 \mathbb{E}_{X_j} (\log P(X_j | X_1 = x_1^i, \dots, X_{j-1} = x_{j-1}^i))) \\
&= \frac{1}{|S|^2} \sum_{s^i \in S} \sum_{j=1}^n (\mathbb{E}_{X_1, \dots, X_{j-1}} (\mathbb{E}_{X_j} (\log^2 P(X_j | X_1 = x_1^i, \dots, X_{j-1} = x_{j-1}^i)) \\
&\quad - \text{Var}_{X_j} (\log P(X_j | X_1 = x_1^i, \dots, X_{j-1} = x_{j-1}^i))) \\
&\quad - \mathbb{E}_{X_1, \dots, X_{j-1}}^2 \mathbb{E}_{X_j} (\log P(X_j | X_1 = x_1^i, \dots, X_{j-1} = x_{j-1}^i))) \\
&= \frac{1}{|S|^2} \sum_{i \in |S|} \sum_{j=1}^n (\mathbb{E}_{X_1, \dots, X_j} (\log^2 P(X_j | X_1 = x_1^i, \dots, X_{j-1} = x_{j-1}^i)) \\
&\quad - \mathbb{E}_{X_1, \dots, X_j}^2 (\log P(X_j | X_1 = x_1^i, \dots, X_{j-1} = x_{j-1}^i))) \\
&\quad - \mathbb{E}_{X_1, \dots, X_{j-1}} \text{Var}_{X_j} (\log P(X_j | X_1 = x_1^i, \dots, X_{j-1} = x_{j-1}^i)) \\
&= \frac{1}{|S|^2} \sum_{i \in |S|} \sum_{j=1}^n (\text{Var}_{X_1, \dots, X_j} (\log P(X_j | X_1 = x_1^i, \dots, X_{j-1} = x_{j-1}^i)) \\
&\quad - \mathbb{E}_{X_1, \dots, X_{j-1}} \text{Var}_{X_j} (\log P(X_j | X_1 = x_1^i, \dots, X_{j-1} = x_{j-1}^i))) \\
&\leq \frac{1}{|S|^2} \sum_{i \in |S|} \sum_{j=1}^n \text{Var}_{X_1, \dots, X_j} (\log P(X_j | X_1 = x_1^i, \dots, X_{j-1} = x_{j-1}^i)) \\
&= \text{Var}_{X_1, X_2, \dots, X_n} \left(\frac{1}{|S|} \sum_{i \in |S|} \log P(s^i) \right)
\end{aligned}$$

□

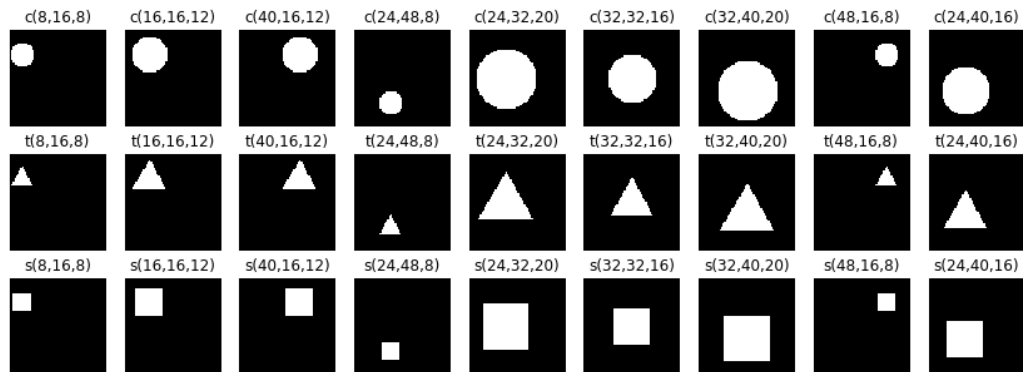


Figure 6: Each shape encoding is on top of the image it represents.

The fifth equation holds from the fact that $\mathbb{E}_X^2 \mathbb{E}_{Y|X}[f(X, Y)] = \mathbb{E}_{X, Y}^2[f(X, Y)]$. The result still stands after applying reweighting for the beam search.

D Shape Encoding Demonstration

In Figure 6, we show the code name on top of the image that it represents. c, s, and t represent circle, square and triangle respectively. The first two numbers represent the position of the shape in the canvas and the last number represents the size.

E Example Outputs and Programs

In Figure 7, we compare the performance of each algorithm qualitatively with one example for each image complexity level. Figure 8 shows some example outputs from the sampling without replacement scheme.

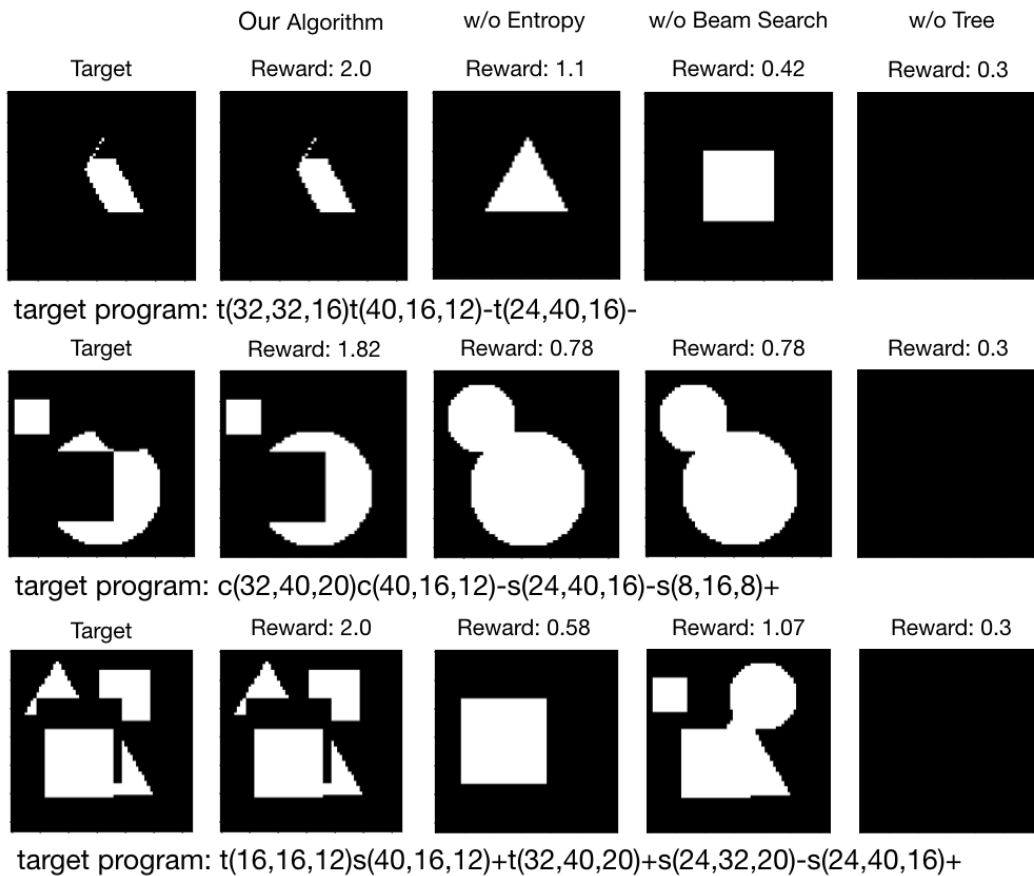


Figure 7: We show a target image from each dataset and attach its correct program below. To the right of the target programs are the outputs for our algorithm and three variants each missing one design feature. The reward is on top of each output image.

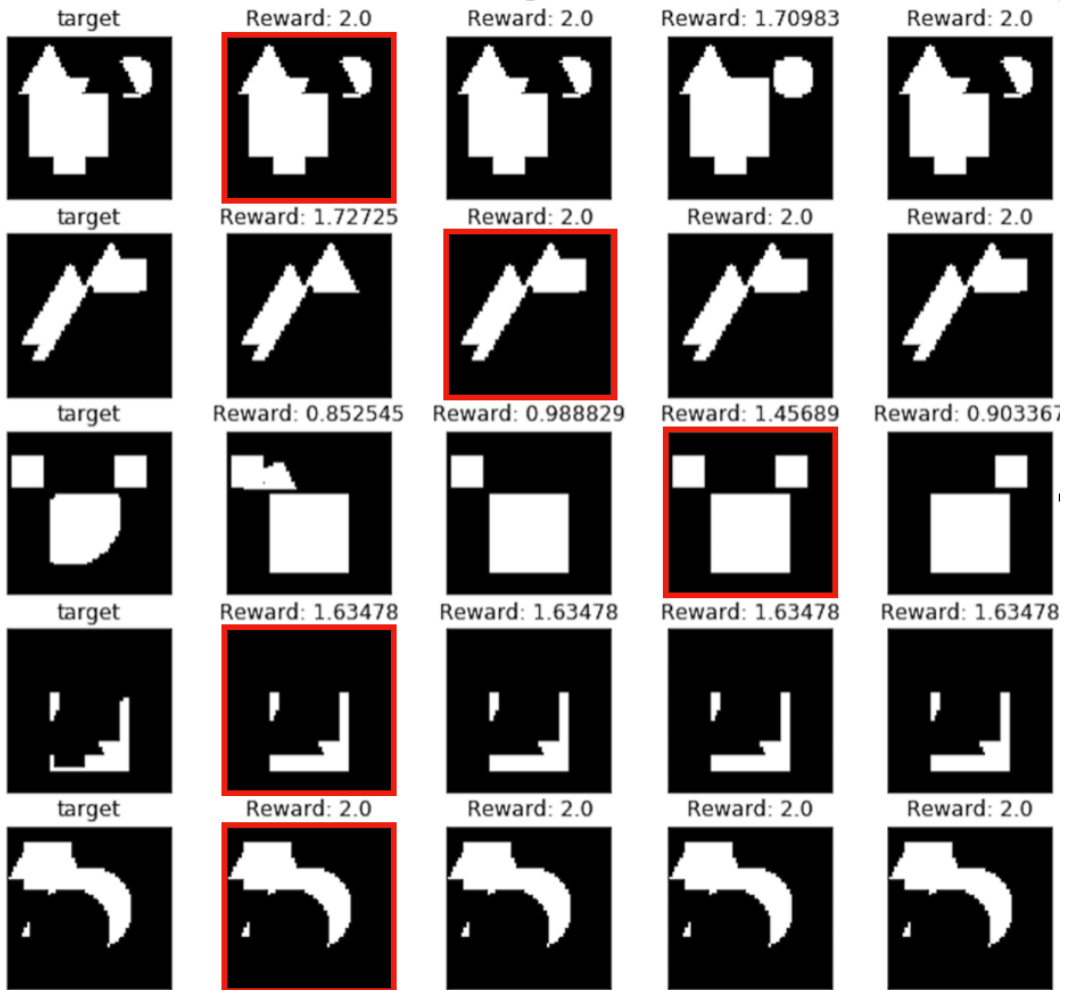


Figure 8: Some example outputs of our algorithm. Each row represents one example occupying 5 columns. The leftmost images of the five columns are the target images and the four columns to its right are the output of four beams. Its corresponding reward is on top of each image. The output is the image with the highest reward among the outputs, which is highlighted in red frame.